

Advanced Scheduling Strategies for Distributed Quantum Computing Jobs

Gongyu Ni¹, Davide Ferrari², Lester Ho¹, and Michele Amoretti^{2,*}

¹*Wireless Communications Laboratory, Tyndall National Institute, Dublin, Ireland*

²*Quantum Software Laboratory, Department of Engineering and Architecture, University of Parma, Parma, 43124 Italy*
(<https://www.qslab.unipr.it/>)

*Corresponding author: Michele Amoretti, michele.amoretti@unipr.it.

Abstract

Scaling the number of qubits available across multiple quantum devices is an active area of research within distributed quantum computing (DQC). This includes quantum circuit compilation and execution management on multiple quantum devices in the network. The latter aspect is very challenging because, while reducing the makespan of job batches remains a relevant objective, novel quantum-specific constraints must be considered, including QPU utilization, non-local gate density, and the latency associated with queued DQC jobs. In this work, a range of scheduling strategies is proposed, simulated, and evaluated, including heuristics that prioritize resource maximization for QPU utilization, node selection based on heterogeneous network connectivity, asynchronous node release upon job completion, and a scheduling strategy based on reinforcement learning with proximal policy optimization. These approaches are benchmarked against traditional FIFO and LIST schedulers under varying DQC job types and network conditions for the allocation of DQC jobs to devices within a network.

Index terms— Distributed quantum computing, Quantum network, Job Scheduling, Makespan, QPU utilization, Non-local gate density

1 Introduction

Distributed quantum computing (DQC) scales the qubit capacity of quantum systems by interconnecting multiple QPUs and enabling collaborative computation. Unlike classical distributed computing, where scaling is typically linear, interconnecting quantum processors yields an exponential increase in computational power [1]. Achieving the DQC paradigm relies on a quantum network infrastructure to cluster multiple quantum processors and effectively increase the available num-

ber of qubits. Communication between remote quantum processors requires the distribution and consumption of EPR pairs over quantum links before any inter-processor operations can be executed. EPR pairs, also denoted as Bell states, are the maximally entangled quantum states of a two-qubit system (i.e., a quantum mechanical system composed of two interacting two-level subsystems) [2, 3].

Transitioning from monolithic to distributed quantum computing introduces challenges in algorithm partitioning and execution management [4]. A quantum compiler is responsible for partitioning a monolithic algorithm into local and remote operations, as in [5, 6]. Execution management, in contrast, focuses on scheduling quantum circuit instances onto the quantum network for each execution round [7].

This paper focuses on execution management. In classical high performance computing, there is a rich literature of algorithms that aim to reduce the makespan of job batches while maximizing the utilization of computational resources [8, 9, 10]. In the DQC domain, execution management is much more challenging because, while reducing the makespan is still a relevant objective, novel quantum-specific constraints must be taken into account. These constraints are mostly related to the generation and distribution of EPR pairs: there is a tradeoff between rate and fidelity (which measures the quality of a quantum state). Furthermore, there is a time limit for consuming an entangled state before decoherence (i.e., loss of quantum information) due to interactions with the environment.

The main contributions of this paper lie in the definition, simulation, and evaluation of scheduling strategies for allocating DQC jobs to networked QPUs. An integrated simulation framework for distributed quantum computation jobs and their execution management was developed. Multiple scheduling strategies, including classical approaches (EPR with node selection, ASAP, and Resource-Prioritize) and a reinforcement learning-based PPO scheduler, were proposed and systemati-

cally evaluated under varying DQC job types and network conditions. The results demonstrate that the EPR scheduler with node selection consistently achieves the highest performance in evaluations, while the PPO scheduler provides a flexible framework guided by reward functions, indicating potential for further optimization through alternative reward strategies.

The paper is organized as follows. In Section 2, related research on scheduling distributed computation tasks in quantum networks and classical distributed systems is reviewed. In Section 3, the framework containing both quantum and network simulations is presented. In Section 4, the performance metrics used to evaluate scheduling methods are introduced. In Section 5, multiple scheduling methods for parallelized and sequentially queued DQC jobs are explained in detail. In Section 6, the simulation settings and the analysis of the results are presented. Finally, Section 7 provides the conclusion of the paper.

2 Related Work

To minimize the total time consumed by quantum and network operations in DQC, the authors of [11] compare and contrast two approaches: a resource-constrained project scheduling (RCPSP) framework with batching and a greedy heuristic algorithm. At each time step, the RCPSP method evaluates which operations are eligible for scheduling based on the availability of quantum resources, such as communication and memory qubits, in order to optimize overall scheduling efficiency.

In [7], the authors formulate the scheduling task as a parallel job-scheduling problem, where a set of jobs with varying processing times must be assigned to multiple machines, with the objective of minimizing the overall schedule length. By estimating DQC job durations using circuit depth (i.e., the number of layers), they propose parallelized FIFO and list-scheduling heuristics and evaluate their performance in terms of makespan, quantum-processor utilization, and network utilization.

In classical distributed computing, scheduling multiple jobs concurrently is an NP-hard problem, including the optimization of the preemptive makespan [8]. Evaluations of distributed computing systems typically consider the execution time of individual and average jobs, as well as fairness across tasks [12].

3 DQC Framework

In this section, the concept of the DQC workflow and the network model, including network link settings and synchronized network simulation, are presented.

3.1 DQC Workflow

The DQC workflow encompasses circuit compilation, decomposition of a monolithic quantum circuit into sub-circuits (each treated as an independent job), and al-

location of Quantum Processing Unit (QPU) nodes to execute these jobs, as illustrated in Figure 1.

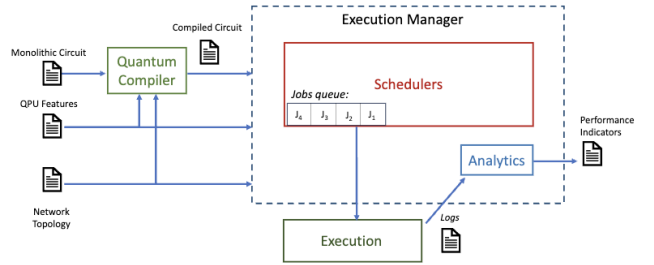


Figure 1: DQC workflow, schedule the sequence of parallelized compiled sub-circuits.

In Figure 1, the Quantum Compiler, as mentioned in [5], is applied to partition the circuit into executable sub-circuits based on the network topology and QPU capabilities, ensuring that inter-node dependencies are minimized. In contrast, the Scheduler manages the execution of these jobs by organizing the job queue and determining whether they should be executed concurrently or sequentially to achieve optimal performance and resource utilization.

In this work, we consider a fully connected QPU network, as a more connected topology reduces the number of required operations. Each QPU is equipped with data qubits and communication qubits and is treated as a node in the network. Links between nodes are heterogeneous, as indicated by the different colors in Figure 2.

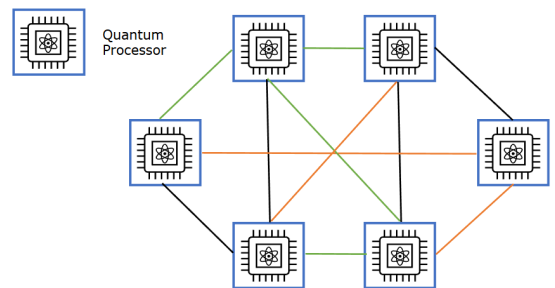


Figure 2: Fully connected QPU network with heterogeneous links.

3.2 Network Model

In the network model, heterogeneous links represent variations in the characteristics of the connections between nodes. Among different scheduling strategies for assigning DQC jobs to available network nodes, the synchronization of arriving jobs within each time slot is also considered.

3.2.1 Heterogeneous links

The performance of links between nodes is characterized by several key parameters, including the entanglement

generation cycle time, expected state delay, entanglement success probability, and fidelity.

In [13], the entanglement success probability P_s represents the probability that a single entanglement generation attempt succeeds. For a link of length d , it can be modeled as

$$P_s(d) = \frac{1}{2} \eta_{\text{penalty}} (\eta_{\text{ion}} \eta_{FC}^{\text{ion} \rightarrow \text{telecom}} \eta_{\text{det}}^{\text{telecom}})^2 10^{-(\alpha/10)(d/2)}, \quad (1)$$

where η_{ion} is the efficiency for emitting and collecting a photon, $\eta_{FC}^{\text{ion} \rightarrow \text{telecom}}$ is the efficiency of frequency conversion from ion to photons, $\eta_{\text{det}}^{\text{telecom}}$ is the detector efficiency for photons at telecom frequency, α is the attenuation factor, and η_{penalty} accounts for a penalty to truncate the detection window.

The cycle time t_{cycle} represents the average duration required for a single entanglement generation attempt. Shorter cycle times enable higher repetition rates and, thus, faster entanglement generation.

The state delay t_{state} represents the expected time to successfully generate an entangled state in a deterministic model and is given by

$$t_{\text{state}} = \frac{t_{\text{cycle}}}{P_s}. \quad (2)$$

Eqn. (2) combines both the time for the entanglement generation attempt and the success probability to quantify the effective time needed to obtain a usable entangled state.

3.2.2 Synchronized Network Simulation

The network layer is modeled with discrete time slots $t = 1, 2, \dots, T$. In each slot, jobs arrive randomly, with the number of jobs following a Poisson distribution $N_t \sim \text{Poisson}(\lambda)$, and they are placed into a queue Q_t . Schedulers immediately receive jobs upon completing the previous queue, allowing the simulation to track execution times and latencies for individual jobs. This setup captures both the stochastic nature of job arrivals and the dynamic resource allocation across the network, enabling a comprehensive evaluation of DQC job scheduling and execution.

4 Performance Metrics

The performance metrics described below are used to evaluate the DQC job schedulers. Makespan indicates the total time consumed to execute an entire queue of DQC jobs, reflecting how efficiently all jobs are completed. QPU utilization and non-local gate density measure how effectively the system uses local quantum resources (data qubits) and quantum network resources (EPR pairs). For overall system assessment, execution-latency performance and fairness metrics are also considered to evaluate both latency and fairness among jobs within the queue.

4.1 Makespan

The makespan M represents the total completion time of a queue of DQC jobs, defined as

$$M = \max_i (t_i^f) - \min_i (t_i^s), \quad (3)$$

where t_i^s and t_i^f denote the start and finish times of the i -th job, respectively. A shorter makespan indicates that the scheduler completes the DQC jobs more efficiently.

4.2 QPU Utilization

The QPU utilization measures the proportion of QPU resources occupied by DQC jobs, normalized by the product of the makespan and the total number of available QPUs.

$$U_{\text{QPU}} = \frac{\sum_i p_i q_i}{M n_{\text{QPU}}} \in [0, 1], \quad (4)$$

where p_i is the execution time of the i -th job, q_i is the number of QPUs required by that job, n_{QPU} is the total number of QPUs in the system, and M is the makespan. A higher QPU utilization indicates that the scheduler uses most of the QPUs in the network at each step.

4.3 Non-Local Gate Density

Non-local gate density quantifies the non-local gates application rate for the arrival DQC job sets. For each job, the start time t_i^s and finish time t_i^f denote the period that the i -th job occupies the resources in the network, with

$$t_i^s = l_i - e_i, \quad t_i^f = l_i, \quad (5)$$

where e_i is the execution time of the job, and l_i is its latency.

The total pairwise overlapping time across all jobs is

$$T_{\text{overlap}} = \sum_{i < j} \max(0, \min(t_i^f, t_j^f) - \max(t_i^s, t_j^s)), \quad (6)$$

while the normalization factor, representing the maximum possible overlap if all intervals were fully overlapping, is

$$T_{\text{max}} = \sum_{i < j} (e_i + e_j). \quad (7)$$

The bounded network utilization is then

$$U_g = \frac{T_{\text{overlap}}}{T_{\text{max}}} \in [0, 1]. \quad (8)$$

A higher U_g indicates that more non-local gates are active simultaneously, reflecting heavier usage of entanglement.

4.4 System Execution-Latency Performance

The Execution-Latency Performance (ELP) of each job j quantifies how close its latency is to the ideal execution time:

$$\text{ELP}_j = \frac{T_{j,e}}{T_{j,l}}, \quad (9)$$

where $T_{j,e}$ is the execution time of job j , and $T_{j,l}$, latency, is the sum of the execution time and the waiting time for the job j in the queue. The ideal value of $\text{ELP}_j = 1$ indicates that the job is executed without waiting.

The System Execution-Latency Performance (SELP) represents the geometric mean of the proportion of execution time and latency for all the jobs:

$$\text{SELP} = \left(\prod_{j=1}^n \text{ELP}_j \right)^{\frac{1}{n}}, \quad (10)$$

where n is the total number of jobs. An ideal $\text{SELP} = 1$ signifies that, on average, all jobs achieve their ideal execution times.

4.5 Fairness Among Jobs

The fairness metric measures the execution times and latencies among jobs, capturing how equally the schedulers affect them:

$$\text{fairness} = 1 - \sigma(\text{ELP}), \quad (11)$$

where σ denotes the standard deviation of ELP_j values. An ideal value of $\text{fairness} = 1$ indicates perfect fairness—i.e., all jobs are executed concurrently in the quantum network.

5 Scheduling Methods

As multiple DQC jobs with varying processing times arrive in each time slot for scheduling across multiple QPUs, schedulers are designed to determine their concurrency and execution order. Given that scheduling in a parallelized queue is NP-hard, schedulers aim to deliver solutions based on their optimization objectives.

5.1 Resource-Prioritize Scheduler

The Resource-Prioritize Scheduler is designed to maximize the utilization of the total available QPU resources. Its scheduling decisions are guided by two criteria. First, it maximizes node utilization, ensuring that as many nodes as possible are actively engaged at each scheduling step. Second, among all the subsets achieving maximal utilization, it prioritizes the jobs with the shortest estimated processing time.

Formally, at each scheduling step, given a set of candidate jobs \mathcal{Q} and a set of available nodes \mathcal{N} , the scheduler

selects a subset $\mathcal{J} \subseteq \mathcal{Q}$ such that

$$\sum_{j \in \mathcal{J}} n_j \leq |\mathcal{N}|. \quad (12)$$

Among all such subsets, it minimizes the total execution time of the parallelized DQC jobs:

$$\min_{\mathcal{J}} \sum_{j \in \mathcal{J}} e_j \quad \text{subject to} \quad \sum_{j \in \mathcal{J}} n_j \text{ is maximal.} \quad (13)$$

This procedure ensures that the scheduler simultaneously maximizes QPU utilization and minimizes execution time at each scheduling step, continuing until all DQC jobs in the current time window have been scheduled.

The pseudo-code is described in Algorithm 1.

Algorithm 1 Resource-Prioritize Scheduler

```

1: Input: job queue  $Q$ , nodes  $\mathcal{N}$ 
2: Output: schedule  $\mathcal{S}$ 
3: for all  $j \in Q$  do
4:   Estimate execution time  $T_j$  and required QPUs  $R_j$ 
5: end for
6: Initialize node availability  $A[n] \leftarrow 0$  for all  $n \in \mathcal{N}$ 
7:  $\mathcal{S} \leftarrow \emptyset$ ,  $\text{round} \leftarrow 0$ 
8: while  $Q \neq \emptyset$  do
9:    $\text{best\_combo} \leftarrow \emptyset$ ,  $\text{best\_util} \leftarrow 0$ ,  $\text{best\_time} \leftarrow \infty$ 
10:  for  $r = 1$  to  $|Q|$  do
11:    for all combinations  $C$  of  $Q$  with size  $r$  do
12:       $R_{\text{tot}} \leftarrow \sum_{j \in C} R_j$ 
13:      if  $R_{\text{tot}} \leq |\mathcal{N}|$  then
14:         $\bar{T} \leftarrow \frac{1}{|C|} \sum_{j \in C} T_j$ 
15:        if  $R_{\text{tot}} > \text{best\_util}$  or ( $R_{\text{tot}} = \text{best\_util}$  and  $\bar{T} < \text{best\_time}$ ) then
16:           $\text{best\_combo} \leftarrow C$ 
17:           $\text{best\_util} \leftarrow R_{\text{tot}}$ 
18:           $\text{best\_time} \leftarrow \bar{T}$ 
19:        end if
20:      end if
21:    end for
22:  end for
23:  for all  $j \in \text{best\_combo}$  do
24:    Remove  $j$  from  $Q$ 
25:  end for
26: end while
27: return  $\mathcal{S}$ 

```

5.2 EPR Scheduler

The EPR Scheduler prioritizes jobs according to their estimated execution time and the entanglement resources they consume, quantified by the number of EPR pairs required. For each job, the scheduler determines its execution time, the number of QPUs needed, and its

EPR usage. The job queue is then reordered in ascending EPR usage, ensuring that jobs requiring fewer non-local entanglement resources are executed earlier. The pseudo-code is described in Algorithm 2.

In contrast to a Resource-Prioritize Scheduler, which aims to maximize QPU utilization at every scheduling step, the EPR Scheduler adopts a more conservative and stability-oriented strategy. It focuses on executing low-EPR, low-latency jobs early rather than saturating node usage. As a result, waiting times for remaining jobs remain relatively low, though overall utilization may not be maximized.

Scheduling proceeds in rounds. In each round, jobs are examined in EPR priority order, and a job is scheduled if a sufficient number of QPUs are available. The job is assigned to a set of unoccupied nodes, its earliest possible start time is computed based on node availability, and all relevant availability values are updated.

Algorithm 2 EPR Scheduler

```

1: Input: job queue  $Q$ , nodes  $\mathcal{N}$ 
2: Output: schedule  $\mathcal{S}$ 
3: for all  $j \in Q$  do
4:   Estimate execution time  $T_j$ , required QPUs  $R_j$ ,
   and EPR usage  $E_j$ 
5: end for
6: Sort  $Q$  in ascending order of  $E_j$ 
7: Initialize node availability  $A[n] \leftarrow 0$  for all  $n \in \mathcal{N}$ 
8:  $\mathcal{S} \leftarrow \emptyset$ ,  $round \leftarrow 0$ 
9: while  $Q \neq \emptyset$  do
10:   $U \leftarrow \emptyset$  {nodes used in this round}
11:  for all  $j \in Q$  do
12:     $k \leftarrow R_j$ 
13:     $\mathcal{C} \leftarrow$  nodes in  $\mathcal{N}$  not in  $U$ 
14:    if  $|\mathcal{C}| < k$  then
15:      continue
16:    end if
17:    for all  $n \in \mathcal{N}_j$  do
18:       $A[n] \leftarrow t_{\text{finish}}$ , add  $n$  to  $U$ 
19:    end for
20:    Remove  $j$  from  $Q$ 
21:  end for
22: end while
23: return  $\mathcal{S}$ 

```

5.3 EPR Scheduler with Node Selection

Given that the EPR scheduler does not consistently achieve full utilization of nodes and links at each scheduling step, and considering that the network exhibits heterogeneous link characteristics, the integration of a node-selection algorithm (Algorithm 3) with the EPR scheduler enhances resource allocation by prioritizing nodes according to their connectivity and network topology.

This ensures that the chosen nodes are connected via the most efficient links, reducing communication overhead and improving scheduling performance.

Algorithm 3 Node-selection algorithm

```

Require: Quantum network graph  $G$ , available nodes
 $\mathcal{N}$ , select  $k$  nodes with minimum total weights
Ensure: Optimal node group  $C^*$ 
1:  $C^* \leftarrow$  None
2:  $\text{min\_weight} \leftarrow \infty$ 
3: for all combinations  $C \subseteq \mathcal{N}$  of size  $k$  do
4:    $\text{weight} \leftarrow 0$ 
5:   for all pairs  $(u, v)$  in  $C$  do
6:      $\text{weight} \leftarrow \text{weight} + G[u][v][\text{weight}]$ 
7:   end for
8:   if  $\text{weight} < \text{min\_weight}$  then
9:      $\text{min\_weight} \leftarrow \text{weight}$ 
10:     $C^* \leftarrow C$ 
11:   end if
12: end for
13: return  $C^*$ 

```

5.4 ASAP Scheduler

In the ASAP scheduling method, nodes are released asynchronously as their assigned jobs complete. Rather than waiting for all nodes to become idle at the end of each scheduling step, as the previous two schedulers do, this scheduler continuously monitors job requirements and node availability, allocating newly freed nodes to pending jobs whenever possible. This dynamic reassignment further improves overall resource utilization across the network, as described in Algorithm 4.

5.5 PPO Scheduler

The reinforcement learning model, Proximal Policy Optimization (PPO) [14], illustrated in Figure 3, is applied to schedule DQC jobs both in parallel and sequentially.

Similar to the other scheduling methods, the environment of the PPO model consists of a set of DQC jobs arriving in each time slot. After receiving these jobs, at each step, the actor of the PPO model attempts to accommodate the jobs with the highest probability as determined by the policy until the resource constraints are met. The actor iterates through these steps until all DQC jobs are scheduled for execution, producing the output for the environment.

Once the environment receives the output from the PPO model, the job sets are executed through the Qoala simulation. This simulation provides the execution and latency time of each job, which are used to compute the reward for each state transition generated by the actor. With full knowledge of the state transitions and rewards stored in the roll-out buffer, the PPO model is trained using a mini-batch size of 64, with updates occurring

Algorithm 4 ASAP Scheduler

```

1: Input: job queue  $Q$ , nodes  $\mathcal{N}$ 
2: Output: schedule  $\mathcal{S}$ 
3: for all  $j \in Q$  do
4:   Estimate execution time  $T_j$  and required QPUs  $R_j$ 
5: end for
6: Initialize  $A[n] \leftarrow 0$  for all  $n \in \mathcal{N}$ ,  $\mathcal{S} \leftarrow \emptyset$ ,  $\text{round} \leftarrow 0$ 
7: while  $Q \neq \emptyset$  do
8:    $\text{scheduled\_round} \leftarrow \emptyset$ ,  $\text{used\_nodes} \leftarrow \emptyset$ 
9:    $\text{round\_start} \leftarrow \min_{n \in \mathcal{N}} A[n]$ 
10:  for all  $j \in Q$  do
11:     $\text{candidate\_nodes} \leftarrow$  free nodes  $\leq \text{round\_start}$ 
    not in  $\text{used\_nodes}$ 
12:    if  $|\text{candidate\_nodes}| \geq R_j$  then
13:       $\text{assigned\_nodes} \leftarrow \text{candidate\_nodes}$ 
14:       $\text{finish} \leftarrow \text{round\_start} + T_j$ 
15:      Record  $(j, \text{assigned\_nodes}, \text{round\_start}, \text{finish})$ 
      in  $\text{scheduled\_round}$ 
16:      for all  $n \in \text{assigned\_nodes}$  do
17:         $A[n] \leftarrow \text{finish}$ 
18:      end for
19:      Add  $\text{assigned\_nodes}$  to  $\text{used\_nodes}$ 
20:      Remove  $j$  from  $Q$ 
21:    end if
22:  end for
23: end while
24: return  $\mathcal{S}$ 

```

every 1024 transitions in the critic network. Using gradient descent on the loss function and the updated advantage estimates, the critic incorporates feedback from the environment and actor actions to update the policy network, enabling better selection of DQC jobs to maximize the reward.

5.5.1 Input Space

At each step, the observation matrix is $S \in \mathbb{R}^{J \times F}$, where J is the maximum number of jobs and F is the feature dimension. Each row corresponds to one job and includes the features of the required number of QPUs n_j , EPR pairs e_j , non-local gates g_j , and the estimated execution time t_j for this job. Formally, the state matrix is defined as:

$$S = \begin{bmatrix} s_1^\top \\ s_2^\top \\ \vdots \\ s_J^\top \end{bmatrix}, \quad s_j = [n_j, e_j, g_j, t_j]. \quad (14)$$

5.5.2 Action

The scheduler employs a multi-selection action space in which the actor chooses a set of jobs to execute in parallel at each step. The action at time t is represented as

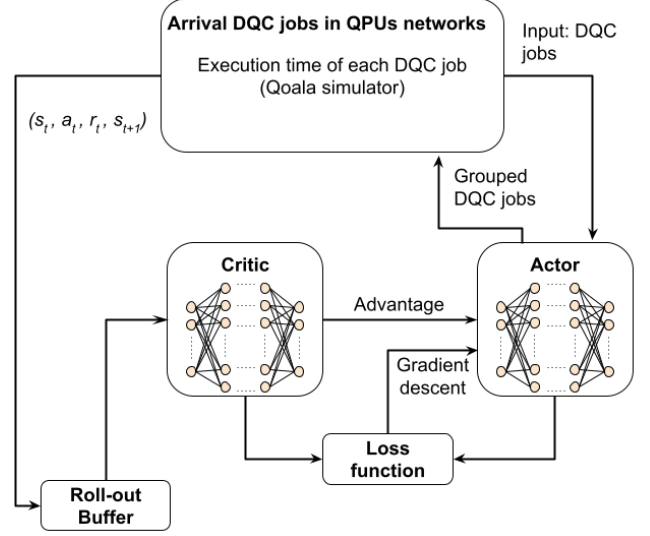


Figure 3: The PPO model contains: environment, state, action, reward and loss function.

a binary vector

$$a^{(t)} = [a_1^{(t)}, a_2^{(t)}, \dots, a_j^{(t)}], \quad a_j^{(t)} \in \{0, 1\}, \quad (15)$$

where $a_j^{(t)} = 1$ indicates that job j is selected. A job can be included in the parallel execution set only if the resource constraint

$$\sum_{j: a_j^{(t)}=1} n_j \leq N_{\max} \quad (16)$$

is satisfied, where N_{\max} denotes the maximum number of QPUs available per scheduling step.

The PPO policy produces logits ℓ_j for all jobs, and the corresponding selection probabilities are given by

$$\pi_\theta(a_j | S) = \frac{\exp(\ell_j)}{\sum_{k=1}^J \exp(\ell_k)}, \quad (17)$$

after masking out jobs that are already selected in the previous steps. The scheduler then selects jobs in decreasing probability order until the resource limit is reached.

5.5.3 Reward

The reward combines a normalized latency penalty with an EPR-aware incentive.

Let e_i and l_i denote the execution time and latency of job i , respectively. Jobs proceed through sequential stages, with the latency of job i in stage s given by

$$l_i = e_i + M_{s-1}, \quad M_{s-1} = \max_{j \in \mathcal{S}_{s-1}} e_j, \quad M_0 = 0. \quad (18)$$

The total latency is

$$L = \sum_{i=1}^n l_i. \quad (19)$$

To obtain a scale-invariant metric, L is normalized by the worst-case serialized latency. Sorting execution times in descending order $e_{(1)} \geq \dots \geq e_{(n)}$, we define

$$L_{\max} = \sum_{k=1}^n (n - k + 1) e_{(k)}, \quad R_{\text{lat}} = \frac{L}{L_{\max}}. \quad (20)$$

PPO Reward For a PPO scheduler without node selection, the quality of QPUs is unknown. To prioritize DQC jobs with low EPR, let d_i be the EPR of job i , γ the inter-stage pressure factor, and

$$D_{s-1} = \max_j d_j, \quad D_0 = 0. \quad (21)$$

The EPR reward is

$$R_{\text{EPR}}^{(1)} = \alpha \frac{1}{n} \sum_s \sum_i \frac{1}{d_i + \gamma D_{s-1}}, \quad (22)$$

where α balances latency and EPR efficiency. High previous-stage EPR (D_{s-1}) increases the denominator, reducing the reward and discouraging sustained high consumption.

The final PPO reward is

$$r^{(1)} = -R_{\text{lat}} + R_{\text{EPR}}^{(1)}. \quad (23)$$

PPO with Node Selection Reward Node selection can shorten execution times for early intra-stage jobs. To further encourage balanced scheduling, we extend the EPR term with intra-stage order. Let o_i denote the execution order of job i within stage s (starting from 0), and β a positional penalty factor:

$$R_{\text{EPR}}^{(2)} = \alpha \frac{1}{n} \sum_s \sum_i \frac{1}{\beta d_i (o_i + 1) + \gamma D_{s-1}}. \quad (24)$$

Jobs scheduled later in a stage (higher o_i) contribute less when their EPR demand is high, promoting low-EPR jobs earlier and improving intra-stage load balancing. The corresponding reward is

$$r^{(2)} = -R_{\text{lat}} + R_{\text{EPR}}^{(2)}. \quad (25)$$

Summary Both rewards penalize high total latency while prioritizing scheduling DQC jobs with lower EPR pairs. With node selection, Eq. 24 further encourages balanced resource usage within each stage.

5.5.4 Loss Function

The PPO model is trained using a total loss \mathcal{L} , a weighted sum of the clipped policy loss, value loss, and entropy bonus:

$$\mathcal{L} = \mathcal{L}_\pi + c_v \mathcal{L}_v - c_e \mathcal{H}, \quad (26)$$

where c_v and c_e are the value and entropy coefficients.

Clipped Policy Loss For the new policy π_θ and the old policy $\pi_{\theta_{\text{old}}}$, the probability ratio is $r_t(\theta) = \pi_\theta(a_t|s_t)/\pi_{\theta_{\text{old}}}(a_t|s_t)$, and the clipped surrogate objective is:

$$\mathcal{L}_\pi = -\mathbb{E}_t \left[\min \left(r_t(\theta) \hat{A}_t, \text{clip}(r_t(\theta), 1 - \epsilon, 1 + \epsilon) \hat{A}_t \right) \right], \quad (27)$$

with \hat{A}_t the advantage estimate and ϵ the clipping parameter.

Value Loss The critic minimizes the MSE between the predicted value $V_\theta(s_t)$ and the target return R_t :

$$\mathcal{L}_v = \mathbb{E}_t \left[(V_\theta(s_t) - R_t)^2 \right]. \quad (28)$$

Entropy Bonus Entropy encourages exploration:

$$\mathcal{H} = \mathbb{E}_t \left[\mathcal{H}(\pi_\theta(\cdot|s_t)) \right]. \quad (29)$$

5.6 Benchmark Schedulers

Below, we provide a brief explanation of the benchmark schedulers from [7].

5.6.1 FIFO Scheduler

In the FIFO scheduler, all quantum processing unit nodes are initially free. Each job is associated with an estimated execution time. Jobs are scheduled strictly in the order of arrival, and each job is assigned to execute at the earliest time when a sufficient number of QPU nodes are available.

5.6.2 LIST Scheduler

The LIST scheduler [8] follows a FIFO ordering of jobs; however, at each time slot, it examines all jobs in the queue to identify the first job that can fit the currently available nodes. This allows some jobs to start earlier than previous jobs if enough nodes are free, thereby improving resource utilization and reducing overall waiting time.

5.7 Schedulers Summary

In summary, as shown in Table 1, the seven scheduling strategies differ in flexibility, resource utilization, and job assignment. FIFO follows a fixed order and has low resource usage, making it simple but unable to group jobs efficiently. LIST introduces flexibility by allowing later jobs to combine, achieving medium utilization while stopping when resources or jobs are exhausted. Resource Priority maximizes resource usage by prioritizing jobs with high resource demand and short estimated times, offering both flexibility and high efficiency.

Schedulers based on EPR focus on minimizing the expected processing requirements. The basic EPR scheduler maintains a fixed order with low utilization, whereas EPR Node Selection improves execution by choosing nodes with good links, all while still using low resources. The PPO scheduler schedules DQC jobs using

the trained PPO model. Finally, the ASAP scheduler dynamically assigns jobs as soon as resources become available, providing high utilization and flexible scheduling while requiring continuous monitoring.

6 Simulation Evaluation

Simulations have been developed and executed using the Qoala Simulator [15], which offers a user-friendly Python API that allows users to mimic both the software and hardware of real quantum network nodes, execute quantum programs, and gather statistics.

6.1 Simulation Settings

In the simulation settings, both the specific DQC jobs and the link parameters applied in the simulation are presented.

6.1.1 DQC Jobs

To compare the scheduling algorithms presented in Section 5, circuits with a number of qubits ranging from 5 to 15 were used. All the considered circuits are of practical interest. They are illustrated briefly below.

GHZ State The Greenberger–Horne–Zeilinger (GHZ) state is an entangled multi-qubit state of the form:

$$|\text{GHZ}_n\rangle = \frac{|0\rangle^{\otimes n} + |1\rangle^{\otimes n}}{\sqrt{2}}. \quad (30)$$

It can be prepared on n qubits by first applying a Hadamard gate to the first qubit, followed by a sequence of CNOT gates connecting the first qubit to all subsequent qubits:

$$|\text{GHZ}_n\rangle = \text{CNOT}_{1,2} \cdots \text{CNOT}_{1,n} H_1 |0\rangle^{\otimes n}. \quad (31)$$

A 5-qubit GHZ circuit using CNOT gates is illustrated schematically in Fig. 4.

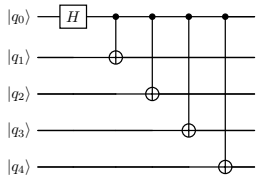


Figure 4: 5-qubit GHZ state preparation. The first qubit is put into superposition via a Hadamard gate, and subsequent qubits are entangled via controlled-NOT operations.

Graph State A graph state associated with a graph $G(V, E)$ is defined as

$$|G\rangle = \left(\prod_{(i,j) \in E} CZ_{i,j} \right) |+\rangle^{\otimes n}, \quad (32)$$

where $n = |V|$ is the number of vertices, each qubit is initialized in the $|+\rangle$ state via Hadamard gates, after which entangling controlled-Z operations are applied for every edge $(i, j) \in E$, as shown in Fig. 5.

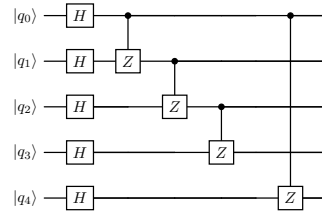


Figure 5: 5-qubit graph state preparation. Each qubit is initialized in the $|+\rangle$ state via a Hadamard gate, and controlled-Z (CZ) gates is introduced according to the edges of the graph.

Quantum Approximate Optimization Algorithm (QAOA)

This algorithm is designed to provide approximate solutions to combinatorial optimization problems. The cost Hamiltonian $\hat{H}_c = \sum_{\alpha} C_{\alpha}$, where C_{α} is the quantum clause Hamiltonian, and a mixer Hamiltonian $\hat{H}_b = \sum_j X_j$, where X_j denotes the Pauli-X operator acting on qubit j [16].

Given a number of rounds $r \geq 1$ and parameter sets $\{\beta_k\}_{k=1}^r$ and $\{\gamma_k\}_{k=1}^r$, the algorithm starts in the uniform superposition $|+\rangle^{\otimes n}$ and alternates the application of the cost and mixer unitaries:

$$U_C(\gamma_k) = e^{-i\gamma_k \hat{H}_c}, \quad (33)$$

$$U_B(\beta_k) = e^{-i\beta_k \hat{H}_b}. \quad (34)$$

This produces the variational state $|\beta, \gamma\rangle$, from which candidate solutions are sampled. The quality of these solutions depends on the chosen depth r and the parameters β, γ .

For the MaxCut problem, the cost Hamiltonian $\hat{H}_c = \sum_{(i,j) \in E} \frac{1}{2}(I - Z_i Z_j)$. An illustrative QAOA circuit for a 5-qubit system on the simple graph with edges $(0, 1)$, $(1, 2)$, $(2, 3)$, $(3, 4)$, and $(0, 4)$ is shown in Fig. 6. Specifically, the rotation gates applied in the quantum circuit are defined as:

$$R_c(\gamma) = \begin{pmatrix} 1 & 0 \\ 0 & e^{-i\gamma} \end{pmatrix}, \quad (35)$$

$$R_b(\theta, \phi, 2\beta) = \begin{pmatrix} \cos(\theta/2) & -e^{2i\beta} \sin(\theta/2) \\ e^{i\phi} \sin(\theta/2) & e^{i(2\beta+\phi)} \cos(\theta/2) \end{pmatrix}. \quad (36)$$

Quantum Fourier Transform (QFT) The Quantum Fourier Transform is defined as in Equation 37:

$$\text{QFT } |x\rangle = \frac{1}{\sqrt{2^k}} \sum_{y=0}^{2^k-1} e^{2\pi i xy/2^k} |y\rangle, \quad (37)$$

Table 1: Summary table of the schedulers.

Scheduler	Features	Order	Resource Usage	End Condition	Update
FIFO	Combine in sequence	Fixed	Low	Next job cannot be grouped	End of parallelized jobs
LIST	Allow later jobs to combine	Flexible	Medium	No jobs or no resources	End of parallelized jobs
Resource-Priority	Prioritize jobs with max resource use and min estimated time	Flexible	High	No jobs or no resources	End of parallelized jobs
EPR	Prioritize jobs with min EPR	Fixed	Low	Next job cannot be grouped	End of parallelized jobs
EPR (Node Selection)	Same as EPR but select nodes with good links	Fixed	Low	Next job cannot be grouped	End of parallelized jobs
PPO	Jobs scheduled by trained model	Flexible	High	No jobs or no resources	End of parallelized jobs
ASAP	Jobs assigned dynamically	Flexible	High	No jobs or no resources	When resources available

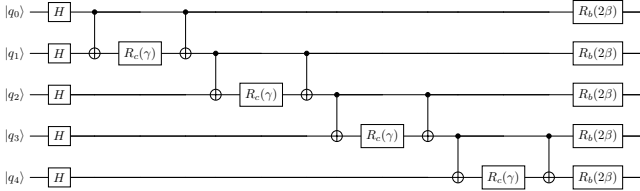


Figure 6: 5-qubit QAOA circuit with one repetition. The cost unitary $U_C(\gamma)$ is implemented via two controlled-NOT and one $R_c(\gamma)$ gates, which is a rotation that depends on the parity of the two qubits. The mixer unitary $U_B(\beta)$ is applied as $R_b(2\beta)$ rotations on all qubits.

where the amplitudes associated with the $|y\rangle$ vectors are the discrete Fourier transforms of the amplitudes of the $|x\rangle$ vectors.

The QFT is implemented recursively, starting with a Hadamard gate applied to the first qubit to create a superposition. Each subsequent qubit is then rotated conditionally using controlled rotations $R_k = \begin{pmatrix} 1 & 0 \\ 0 & e^{2\pi i/2^k} \end{pmatrix}$ on the target qubit. A schematic 5-qubit QFT circuit is shown in Fig. 7.

Variational Quantum Eigen-solver (VQE) This is a hybrid quantum-classical algorithm designed to approximate the ground state energy of a given Hamiltonian \hat{H} , as described in Ref. [16]. A variational state $|\psi(\theta_i)\rangle$ is prepared with parameters θ_i , chosen such that the number of parameters scales linearly with the system size. The expectation value of the Hamiltonian is

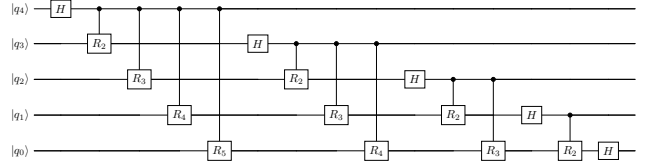


Figure 7: 5-qubit QFT circuit with controlled-phase rotations R_k . Hadamard gates initialize superpositions, and controlled-phase gates implement the Fourier transform phases.

calculated on a quantum computer as

$$E = \frac{\langle \psi(\theta) | \hat{H} | \psi(\theta) \rangle}{\langle \psi(\theta) | \psi(\theta) \rangle}. \quad (38)$$

The parameters θ_i are updated using a classical nonlinear optimizer.

In this paper, EfficientSU2 is used, for which each qubit is first rotated using parameterized R_Y and R_Z gates with parameters randomly initialized in $[0, 2\pi]$. Entanglement is applied linearly, such that controlled-NOT gates connect each qubit to its nearest neighbor sequentially. A schematic representation of a single-layer 5-qubit VQE is shown in Fig. 8.

6.1.2 Job Selection Distribution

In the simulation, the initial job list used for random selection is kept fixed and is ordered from the job with the smallest number of non-local gates to the one with the largest. However, not only is the network load varied, but the probability of selecting each job is also varied, which is referred to as the varied job selection distribution.

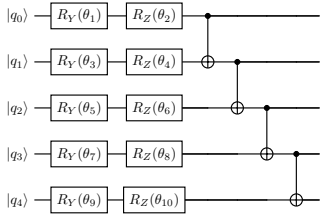


Figure 8: 5-qubit VQE circuit using linear nearest-neighbor entanglement with one repetition. Each qubit undergoes parameterized R_Y and R_Z rotations, followed by controlled-NOT gates between nearest neighbors. The rotation parameters θ_i are randomly initialized in $[0, 2\pi]$.

A non-uniform sampling distribution is imposed over the set of jobs $\mathcal{J} = \{J_1, J_2, \dots, J_n\}$. Each job J_i is assigned a weight

$$w_i = i^\alpha, \quad i = 1, \dots, n, \quad (39)$$

where $\alpha \in [0, 1]$ controls the degree of bias. When $\alpha = 0$, uniform weighting is obtained, whereas linear weighting is obtained when $\alpha = 1$.

The sampling probabilities are obtained by normalizing these weights:

$$p_i = \frac{w_i}{\sum_{j=1}^n w_j}. \quad (40)$$

Thus, the more biased the job selection distribution, the more likely the random selection will choose jobs with a higher number of non-local gates. This is because jobs closer to the end of the list have a higher probability of being selected according to Eq. (40).

6.1.3 Link Parameters

As discussed in Section 3.2.1, the heterogeneous links are modeled by Eq. (1). According to [13], the parameters in the equation are summarized in Table 2, where $\eta_{\text{penalty}} = 0.12$ corresponds to a fidelity of 0.88, and $\eta_{\text{penalty}} = 0.20$ corresponds to a fidelity of 0.95. We recall that the fidelity F quantifies the quality of the generated entangled state relative to an ideal Bell pair, with higher fidelity indicating a state closer to the desired maximally entangled state.

Table 2: Link parameters for a trapped-ion link at 0.1 km.

	$\eta_{FC}^{\text{ion} \rightarrow \text{telecom}}$	$\eta_{\text{det}}^{\text{telecom}}$	η_{penalty}	η_{ion}	α	$d(\text{km})$
Bad	0.5	0.75	0.12	0.87	0.2	0.1
Medium	0.5	0.75	0.20	0.87	0.2	0.1
Good	0.7	0.90	0.20	0.87	0.2	0.1

Applying the parameters in Table 2 and the t_{cycle} in Eq. (2) yields the entanglement success probability P_s , the fidelity of the generated entangled pairs, and the

state delay shown in Table 3, which summarizes these quantities for the three representative trapped-ion link configurations.

Table 3: Performance parameters for trapped-ion links.

Link quality	Cycle time (ns)	P_s	F	State delay (ns)
Bad	1.8×10^6	6.37×10^{-3}	0.88	2.83×10^8
Medium	1.0×10^6	1.06×10^{-2}	0.95	9.42×10^7
Good	2.0×10^5	2.99×10^{-2}	0.95	6.67×10^6

6.2 Results

The simulation results of the classical schedulers are analyzed using the performance metrics described in Section 4. The results for the PPO scheduler, evaluated under the specified simulation settings with a fixed number of 5 DQC jobs per time slot, are analyzed at the end.

6.2.1 Makespan

Although network load and job distribution vary across simulation settings, the scheduler that consistently achieves the lowest makespan is the EPR scheduler with node selection, as shown in Fig. 9. The EPR scheduler prioritizes DQC jobs that require fewer EPR pairs, which reduces the waiting time for the remaining jobs, as tasks with fewer EPR pairs generally exhibit shorter execution times. Furthermore, the node selection algorithm exploits information about heterogeneous links in the network. Although not all QPUs are fully utilized at every scheduling stage, selecting QPUs connected by higher-quality links reduces the time required for entanglement generation and state preparation.

The scheduler with the second-lowest makespan is the ASAP scheduler. It is designed to allocate QPUs as soon as one of the DQC jobs finishes and a free QPU becomes available for a remaining job. Its mechanism enables more dynamic job selection by utilizing idle QPUs immediately, rather than relying on a statically determined set of parallelized jobs.

With respect to the remaining schedulers, EPR, Resource-Priority, FIFO, and LIST, their performance in makespan is largely similar, as shown in Table 4.

6.2.2 QPU Utilization

Figure 10a exhibits the cumulative probability of QPU utilization per time slot under different scheduling methods. Compared with Fig. 10a and Fig. 10c, the differences at network load 8 are more pronounced. FIFO achieves the lowest QPU utilization, whereas Resource-Priority achieves the highest. This is because QPU utilization reflects both the number of QPUs and their occupation time relative to the makespan of incoming DQC job sets. Consequently, the Resource-Priority scheduler shows a clear advantage in maximizing QPU utilization within the quantum network.

When comparing results with and without bias toward DQC jobs that consume more EPR pairs, the perfor-

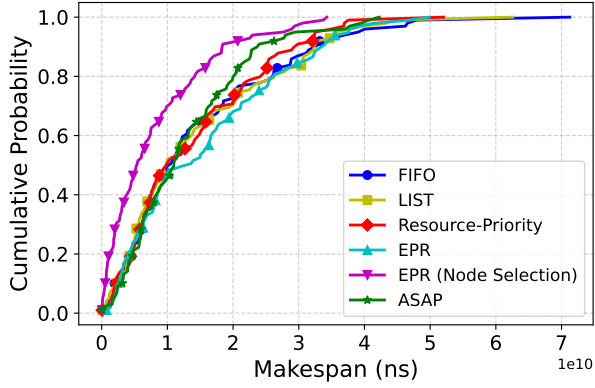
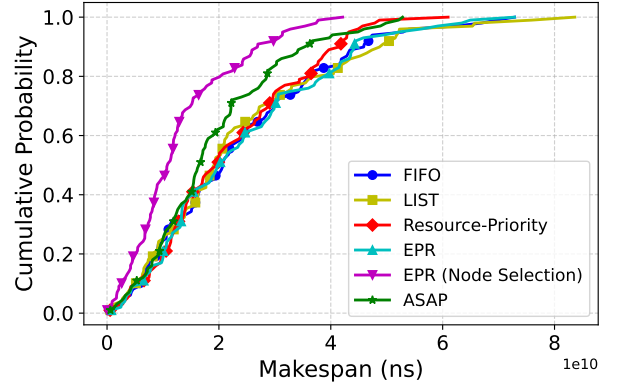
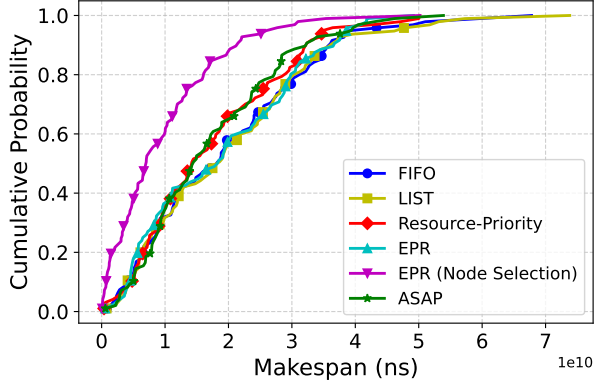
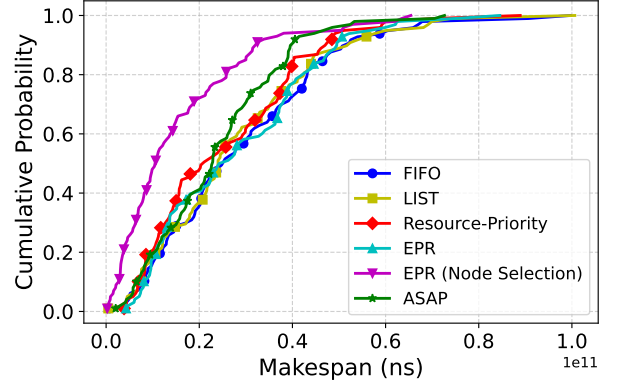
(a) Network load $\lambda = 5$.(b) Network load $\lambda = 8$.(c) Network load $\lambda = 5$, with biased parameter $\alpha = 0.5$ for the job selection.(d) Network load $\lambda = 8$, with biased parameter $\alpha = 0.5$ for the job selection.

Figure 9: The cumulative probability of makespan in each time slot among different schedulers.

Table 4: Average Makespan (ns) under different network settings.

Network settings	FIFO	LIST	Resource-Priority	EPR	EPR (Node Selection)	ASAP
$\lambda = 5$	14727052862.12	14606378120.20	13777802195.05	15662064210.41	8200559162.42	12899515063.33
$\lambda = 5$, bias $\alpha = 0.5$	19536516373.21	19964812591.79	17280297619.23	18624804790.10	9691087657.73	17184282443.30
$\lambda = 8$	23552383801.92	23531843813.23	21863926134.10	23800765245.50	13009064082.02	19024407394.80
$\lambda = 8$, bias $\alpha = 0.5$	29043634426.65	27883862862.40	25442004486.06	27888684040.26	15505274707.30	23856469763.99

mance gap among scheduling methods becomes smaller when bias is included, as shown in Fig. 10c and Fig. 10d.

In Table 5, the highest mean utilization at network load 5 is achieved by the Resource-Priority and ASAP schedulers. As the network load increases and DQC jobs become more complex, the advantages of the Resource-Priority and EPR schedulers with node selection become increasingly evident.

6.2.3 Non-Local Gate Density

Non-Local Gate Density quantifies the overlap of each job's occupation with other jobs. Since the non-local gate is assumed to dominate the execution time, a higher overlap in execution time indicates greater reliance on the entanglement for the non-local gate. Conversely, lower values are preferable.

In Table 6, under varying network settings, the FIFO

scheduler exhibits the lowest non-local gate density among all scheduling methods, as it strictly follows the request order, resulting in sparse DQC job distribution at each step.

The second lowest is the EPR scheduler with node selection. This is because EPR scheduling is relatively sparse at each step, and the execution time per job in the EPR scheduler with node selection is relatively small, as it tends to utilize high-quality links when executing DQC jobs.

6.2.4 System Execution-Latency Performance and Fairness

Unlike previous evaluations of Makespan, QPU utilization, and Non-Local Gate Density, which quantify the overall performance of arriving DQC job sets, the System Execution-Latency Performance (SELP) and Fair-

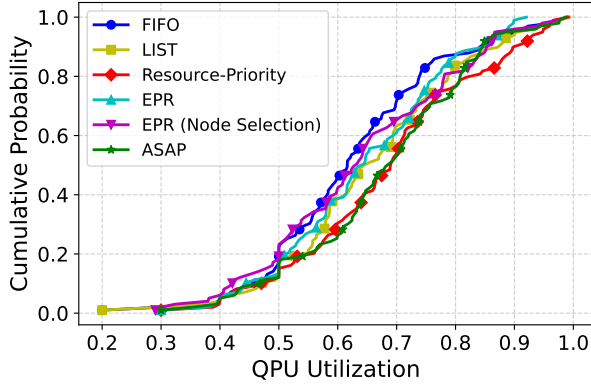
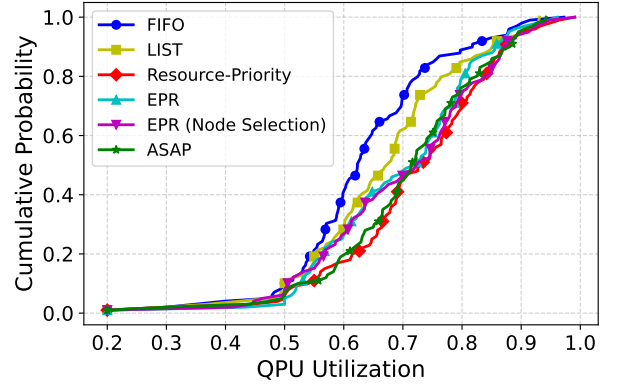
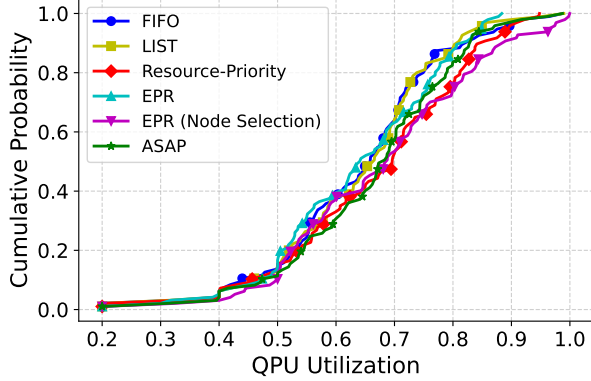
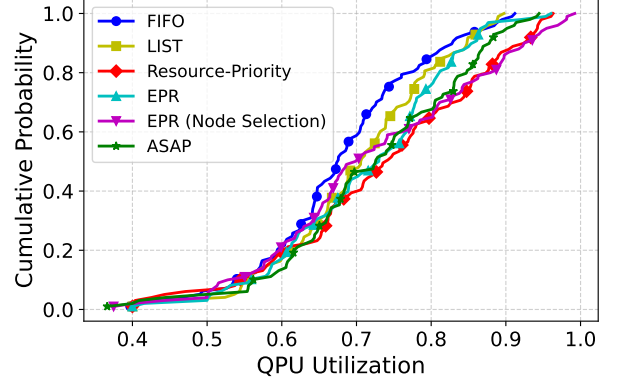
(a) Network load $\lambda = 5$.(b) Network load $\lambda = 8$.(c) Network load $\lambda = 5$, with biased parameter $\alpha = 0.5$ for the job selection.(d) Network load $\lambda = 8$, with biased parameter $\alpha = 0.5$ for the job selection.

Figure 10: The cumulative probability of QPU utilization in each time slot among different schedulers.

Table 5: Average QPU utilization under different network settings.

Network settings	FIFO	LIST	Resource-Priority	EPR	EPR (Node Selection)	ASAP
$\lambda = 5$	0.6278	0.6592	0.6849	0.6460	0.6394	0.6779
$\lambda = 5$, bias $\alpha = 0.5$	0.6404	0.6412	0.6700	0.6389	0.6800	0.6660
$\lambda = 8$	0.6373	0.6669	0.7198	0.6945	0.7018	0.7084
$\lambda = 8$, bias $\alpha = 0.5$	0.6802	0.7028	0.7347	0.7140	0.7245	0.7240

ness metrics assess the performance of individual DQC jobs within the queue arranged by the schedulers.

The Execution-Latency Performance (ELP) indicates a job's execution efficiency relative to its latency. A value closer to 1 implies reduced waiting time for that job, which is desirable. However, due to the limited number of QPUs in the network, not all DQC jobs can be executed in parallel. Therefore, both SELP and fairness among jobs are important, with higher values indicating better performance. The schedulers' SELP performance and fairness for each time slot are shown in Table 7 and Table 8 respectively.

Both the EPR scheduler and the EPR scheduler with node selection achieve the highest SELP and fairness. This is because they prioritize jobs with shorter execution times and assign them to high-quality links, thereby

avoiding prolonged execution that would result from scheduling on lower-quality links.

The second-best performance is observed with the Resource Priority scheduler, particularly under high network load, which achieves relatively high SELP and low unfairness compared to the other schedulers. This is due to its strategy of compacting as many jobs as possible while prioritizing combinations that consume fewer EPR pairs.

It is important to note that the SELP and fairness of the ASAP scheduler exhibit variability similar to benchmark methods such as LIST and FIFO. This is expected, as ASAP is designed solely to dynamically utilize spare QPUs rather than optimize execution-latency performance or fairness.

Table 6: Average non-local gate density under different network settings.

Network settings	FIFO	LIST	Resource-Priority	EPR	EPR (Node Selection)	ASAP
$\lambda = 5$	0.1396	0.1504	0.1560	0.1425	0.1318	0.1541
$\lambda = 5$, bias $\alpha = 0.5$	0.1134	0.1148	0.1228	0.1143	0.1264	0.1213
$\lambda = 8$	0.0711	0.0814	0.0906	0.0837	0.0816	0.0870
$\lambda = 8$, bias $\alpha = 0.5$	0.0811	0.0884	0.0913	0.0853	0.0843	0.0888

Table 7: Average SELP under different network settings.

Network settings	FIFO	LIST	Resource-Priority	EPR	EPR (Node Selection)	ASAP
$\lambda = 5$	0.6793	0.7188	0.7794	0.8711	0.8245	0.6868
$\lambda = 5$, bias $\alpha = 0.5$	0.7288	0.7475	0.7812	0.8785	0.8012	0.6679
$\lambda = 8$	0.4977	0.5405	0.6749	0.7541	0.6880	0.4980
$\lambda = 8$, bias $\alpha = 0.5$	0.5183	0.5433	0.6613	0.7778	0.7285	0.4612

6.2.5 PPO Scheduler Performance

Due to the input space limitation of the proposed PPO model for the PPO scheduler, only a fixed number of DQC jobs can arrive per time slot. This limitation can be mitigated by training multiple models with different fixed numbers of jobs. For simplicity, this paper presents the results of a single trained PPO model with 5 DQC jobs per time slot, compared with previously proposed classical schedulers.

In Table 9, PPO is trained to prioritize DQC jobs with lower EPR-pair requirements, resulting in behavior similar to that of the EPR scheduler. However, the additional latency-penalization term enables the model to learn from the training data and potentially outperform the EPR scheduler.

In terms of latency, PPO (with and without node selection) achieves similar or slightly lower values compared to the EPR scheduler. For QPU utilization and Non-Local Gate Density, PPO variants perform slightly better, as indicated by their lower values relative to EPR and EPR with node selection, respectively. For SELP and Fairness, PPO performs slightly worse than its EPR counterparts, reflected by comparatively lower metric values.

7 Conclusion

This paper establishes an integrated model for simulating distributed quantum computation (DQC) jobs and their execution management. To manage these DQC jobs at the quantum network layer, multiple schedulers are proposed and evaluated.

The EPR scheduler with node selection achieves the lowest makespan, the highest system execution-latency performance, and the greatest fairness across various network loads and job type distributions. The ASAP scheduler performs second best in terms of makespan, while the Resource-Prioritize scheduler achieves the highest QPU utilization. Unlike the classical schedulers discussed above, the PPO scheduler is guided by a reward function. In future work, additional reward strategies could be explored to further influence the behavior

of the PPO scheduler.

Data Availability

All data and code required to reproduce all plots shown herein are available at <https://zenodo.org/records/18802413>.

Acknowledgements

This work was funded by the European Union’s Horizon Europe research and innovation programme under grant agreement No. 101102140 – QIA Phase 1. Furthermore, this work benefited from the High Performance Computing facility at the University of Parma, Italy.

References

- [1] A. S. Cacciapuoti, M. Caleffi, F. Tafuri, F. S. Cataliotti, S. Gherardini, G. Bianchi, Quantum internet: Networking challenges in distributed quantum computing, *IEEE Network* 34 (1) (2019) 137–143.
- [2] N. Brunner, D. Cavalcanti, S. Pironio, V. Scarani, S. Wehner, Bell nonlocality, *Rev. Mod. Phys.* 86 (2014) 419–478. doi:10.1103/RevModPhys.86.419. URL <https://link.aps.org/doi/10.1103/RevModPhys.86.419>
- [3] M. Amoretti, S. Carretta, Entanglement verification in quantum networks with tampered nodes, *IEEE Journal on Selected Areas in Communications* 38 (3) (2020) 598–604. doi:10.1109/JSAC.2020.2967955.
- [4] M. Caleffi, M. Amoretti, D. Ferrari, J. Illiano, A. Manzalini, A. S. Cacciapuoti, Distributed quantum computing: a survey, *Computer Networks* 254 (2024) 110672.
- [5] D. Ferrari, S. Carretta, M. Amoretti, A modular quantum compilation framework for distributed quantum computing, *IEEE Transactions on Quantum Engineering* 4 (2023) 1–13.

Table 8: Average Fairness under different network settings.

Network settings	FIFO	LIST	Resource-Priority	EPR	EPR (Node Selection)	ASAP
$\lambda = 5$	0.7740	0.7914	0.8212	0.8786	0.8452	0.7777
$\lambda = 5$, bias $\alpha = 0.5$	0.7928	0.7985	0.8114	0.8843	0.8258	0.7594
$\lambda = 8$	0.6902	0.7020	0.7500	0.8018	0.7545	0.6871
$\lambda = 8$, bias $\alpha = 0.5$	0.7084	0.7067	0.7502	0.8203	0.7805	0.6804

Table 9: Average value of Schedulers' performance metrics when 5 DQC jobs arrive at each time slot.

Scheduler	Makespan (ns)	QPU Utilization	Non-Local Gate Density	SELP	Fairness
FIFO	14890769534.75	0.6307	0.1068	0.6681	0.7441
LIST	13974889377.40	0.6563	0.1229	0.7090	0.7623
Resource-Priority	14680975010.60	0.6905	0.1312	0.7459	0.7811
EPR	15639021779.25	0.6860	0.1267	0.8837	0.8786
EPR (Node Selection)	11093070329.54	0.6634	0.1098	0.8469	0.8505
ASAP	13072450278.20	0.6902	0.1250	0.6333	0.7116
PPO	16021685244.95	0.6644	0.1213	0.8016	0.8183
PPO (Node Selection)	9031417532.07	0.6400	0.1018	0.7816	0.8136

- [6] X. Xu, Y. Liu, Y. Mao, Y. Yang, Remote gate scheduling in distributed quantum computing, in: 2025 IEEE 45th International Conference on Distributed Computing Systems (ICDCS), IEEE, 2025, pp. 846–856.
- [7] D. Ferrari, M. Bandini, M. Amoretti, Execution management of distributed quantum computing jobs, in: 2024 IEEE International Conference on Quantum Computing and Engineering (QCE), Vol. 2, IEEE, 2024, pp. 150–154.
- [8] B. Johannes, Scheduling parallel jobs to minimize the makespan, *Journal of Scheduling* 9 (5) (2006) 433–452.
- [9] R. A. Dutton, W. Mao, J. Chen, W. Watson, Parallel job scheduling with overhead: A benchmark study, in: 2008 international conference on networking, architecture, and storage, IEEE, 2008, pp. 326–333.
- [10] J. Sgall, G. J. Woeginger, Multiprocessor jobs, preemptive schedules, and one-competitive online algorithms, in: *International Workshop on Approximation and Online Algorithms*, Springer, 2014, pp. 236–247.
- [11] N. K. Chandra, E. Kaur, K. P. Seshadreesan, Network operations scheduling for distributed quantum computing, in: 2024 IEEE 6th International Conference on Trust, Privacy and Security in Intelligent Systems, and Applications (TPS-ISA), IEEE, 2024, pp. 506–515.
- [12] M. Isard, V. Prabhakaran, J. Currey, U. Wieder, K. Talwar, A. Goldberg, Quincy: fair scheduling for distributed computing clusters, in: *Proceedings of the ACM SIGOPS 22nd symposium on Operating systems principles*, 2009, pp. 261–276.
- [13] S. Oslovich, B. van der Vecht, S. Wehner, Compilation strategies for quantum network programs using qoala, arXiv preprint arXiv:2505.06162.
- [14] J. Schulman, F. Wolski, P. Dhariwal, A. Radford, O. Klimov, Proximal policy optimization algorithms, arXiv preprint arXiv:1707.06347.
- [15] B. van der Vecht, A. T. Yücel, H. Jirovská, S. Wehner, Qoala: an application execution environment for quantum internet nodes, arXiv preprint arXiv:2502.17296.
- [16] A. Adedoyin, J. Ambrosiano, P. Anisimov, W. Casper, G. Chennupati, C. Coffrin, H. Djidjev, D. Gunter, S. Karra, N. Lemons, et al., Quantum algorithm implementations for beginners, arXiv preprint arXiv:1804.03719.